Naphthalene Imide Dimer as Interface Engineering: An Efficient Strategy for Achieving High-Performance Perovskite Solar Cells

Helin Wang[a,b], Fan Zhang[a], Zhuohua Li[d], Junmin Zhang[d], Jiarong Lian[a], Jun Song[a,*], Junle Qu[a], Wai-Yeung Wong[b,c,*]

[a] Key Laboratory of Optoelectronic Devices and Systems of Ministry of Education and Guangdong Province, College of Physics and Optoelectronic Engineering, Shenzhen University, Shenzhen 518060, Guangdong, P. R. China.

[b] Department of Applied Biology and Chemical Technology, The Hong Kong Polytechnic University, Hung Hom, Kowloon, Hong Kong, P. R. China.

[c] The Hong Kong Polytechnic University Shenzhen Research Institute, Shenzhen 518057, P. R. China.

[d] College of Chemistry and Environmental Engineering, Shenzhen University, Nanshan District, Shenzhen 518060, Guangdong, P. R. China.

* Corresponding authors.

E-mail: songjun@szu.edu.cn (J. Song), wai-yeung.wong@polyu.edu.hk (W.-Y. Wong).

Keywords: naphthalene imide; interface engineering; surface passivation; electron extraction; perovskite solar cell.

Abstract: How to design and synthesize interfacial engineered materials that have efficient surface passivation and electron extraction properties is an important problem in the field of optoelectronic materials. Herein, a simple naphthalene imide dimer, namely 2FBT2NDI, is developed by Stille coupling reaction with a high yield, and it is used as interface engineering for inverted perovskite solar cells (PSC). Owing to the existence of intermolecular interactions between $MAPbI_3$ and the 2FBT2NDI layer, the introduction of the interfacial

layer can passivate the surface defects of perovskite film and improve interface contact. In addition, 2FBT2NDI exhibits suitable energy levels and high electron mobility because of its large linear conjugated skeleton containing two fluorine atoms, which are beneficial for electron extraction for efficient PSCs. Employing 2FBT2NDI as an interfacial layer, inverted PSCs show a maximum power conversion efficiency of 20.1%, which is over 14% higher than that of the control devices without interfacial layer (17.1%). These results highlight that the naphthalene imide dimer can potentially be used as a commercializable interfacial material for achieving high-performance PSCs.

1. Introduction

Perovskite solar cells (PSCs) have attracted wide attention of researchers in the photovoltaic field because of high power conversion efficiency (*PCE*) and great potential for commercialization [1]. The addition of the electron transport layer (ETL) and hole transport layer in PSCs enhances the directional charge transport of perovskite materials and reduces the charge recombination to improve the device performance [2, 3]. Therefore, the exploration of hole transport and electron transport materials play a crucial role in the development of the PSCs [4]. As far as we know, metal oxides and fullerene derivatives are commonly used as the electron transport materials in PSCs. However, using metal oxides as the ETL, their low electrical conductivity and lots of film surface defects will greatly affect the charge transporting properties. Additionally, PCBM is a fullerene derivative and has disadvantages such as insufficient perovskite film coverage and poor chemical stability [5, 6]. The hydrophilic nature of the ester group of PCBM could accelerate the destruction of perovskite by water under ambient condition [7]. Therefore, there is the addition of interfacial layer between perovskite and PCBM layer to modify perovskite film and enhance electron extraction, which can make up for the shortcoming of PCBM. Furthermore, high-efficiency

electron transport materials (metal oxides and PCBM) have a relatively single function, and only electron transport cannot improve interface contact or passivate the surface defects of perovskite films, which is not conducive to further improving the device performance and stability [8]. Therefore, there is a strong motivation to design and synthesize commercializable interfacial materials that have enhanced electron extraction and efficient surface passivation.

Naphthalene diimides (NDI) derivatives are classic organic dyes that are widely used as the electron transport materials in organic solar cells [9-11], organic light-emitting diodes [12, 13], and organic field effect transistors [14, 15]. However, NDI derivatives have small conjugated skeleton, resulting in unsuitable LUMO levels and low electron mobilities [16, 17]. When they are used as the ETLs, these disadvantages cause energy level barrier and make them difficult to achieve efficient electron injection and transport. Therefore, the development of NDI derivatives with suitable energy levels and high electron mobility has attracted significant attention in the optoelectronic material field. Benzothiadiazole-dithiophene is a classic electron-withdrawing group that is usually used to construct organic semiconductors with larger conjugated framework [18, 19]. It also contains several nitrogen and sulfur atoms, easily generating hydrogen bonds and strong intermolecular interactions, which could passivate the surface defects of perovskite films. Therefore, our interest is developing NDI derivatives with benzothiadiazole-dithiophene unit as a novel interfacial engineered material for efficient inverted PSCs. However, owing to the unsuitable energy levels and low electron transport property, the NDI derivative containing benzothiadiazole-dithiophene unit shows poor photovoltaic performance [20]. Hence, we have developed the NDI dimer with bisfluorobenzothiadiazole-dithiophene conjugated framework (2FBT2NDI) to solve the above problem. On the one hand, fluorine is a strong electron-withdrawing atom that can effectively lower the molecular energy levels and helps to improve charge extraction and transport. On

the other hand, the fluorine atom, the most electronegative element, could form the hydrogen bonds and strong intermolecular interactions, which is beneficial for passivating the perovskite surface defects and suppressing recombination losses. In addition, 2FBT2NDI can be prepared by a simple synthetic route with a high yield, and such a simple molecular structure has a better chance for achieving commercial production.

Herein, 2FBT2NDI was synthesized by the simple Stille coupling reaction with a high yield. Furthermore, 2FBT2NDI has a large linear conjugated skeleton, and the introduction of two fluorine atoms and benzothiadiazole-dithiophene unit can regulate the energy levels and enhance intermolecular interactions, which allow the molecule to exhibit good thermal stability and high electron mobility. Thus, 2FBT2NDI was utilized as interface engineering for inverted PSCs in this research to passivate the $MAPbI_3$ surface defects and to improve the electron extraction and transport. Compared with the control device without 2FBT2NDI, the addition of the 2FBT2NDI as the interfacial layer effectively improved the electron extraction, suppressed the charge-trapped recombination at the perovskite/ETL interface, reduced the hysteresis effect, and improved the device performance. After optimization, the efficiency of the device with the interfacial layer reached to 20.1%, which demonstrated that 2FBT2NDI is a highly efficient interfacial engineered material with great potential in the photovoltaic field.

2. Experimental Section

2.1. Synthesis of compound Br-NDI

Br-NDI: 4-Bromo-1,8-naphthalic anhydride (5 g, 18.05 mmol) and 3-aminopentane (12.6 mL, 0.108 mol) were added to 50 mL dry ethylene glycol and stirred at 100 ^{o}C under an argon atmosphere. After 10 hours, the reaction was cooled to room temperature. Then the mixture was poured into 50 mL water, and extracted with 30 mL of dichloromethane three times. The combined organic layer was washed with brine, dried over magnesium sulphate, and concentrated. The crude product was purified by silica gel column chromatography with

petroleum ether:dichloromethane (2:1, v/v) as eluent to obtain Br-NDI (81%, 5.06 g, 14.62 mmol). ^{1}H NMR (400 MHz, $CDCl_3$, 25 ºC, δ) : 8.64-8.63 (d, 1H, Ar H), 8.56-8.54 (d, 1H, Ar H), 8.40-8.38 (d, 1H, Ar H), 8.04-8.02 (d, 1H, Ar H), 7.86-7.82 (t, 1H, Ar H), 5.05-5.00 (m, 1H, CH), 2.29-2.17 (m, 2H, CH_2), 1.96-1.85 (m, 2H, CH_2), 0.92-0.85 (t, 6H, CH_3).

2.2. Synthesis of compound 2FBT2NDI

2FBT2NDI: Br-NDI (0.2 g, 0.58 mmol), 2FBT (0.15 g, 0.23 mmol), $Pd_2(dba)_3$ (54 mg, 0.058 mmol) and tris(2-methylphenyl)-phosphine (76 mg, 0.23 mmol) were added to 15 mL dry toluene and stirred at 110 ºC under an argon atmosphere. After 12 hours, the solvent was stripped off by a rotary evaporator, and the crude product was purified by silica gel column chromatography with petroleum ether:dichloromethane (1:2, v/v) as eluent to obtain 2FBT2NDI (82%, 0.16 g, 0.19 mmol). ^{1}H NMR (400 MHz, $CDCl_3$, 25 ºC, δ) : 8.74-8.72 (d, 2H, Ar H), 8.68-8.63 (t, 4H, Ar H), 8.46-8.45 (d, 2H, Ar H), 7.98-7.96 (d, 2H, Ar H), 7.85-7.80 (t, 2H, Ar H), 7.54-7.53 (d, 2H, Ar H), 5.10-5.07 (m, 2H, CH), 2.30-2.26 (m, 4H, CH_2), 1.96-1.92 (m, 4H, CH_2), 0.95-0.91 (t, 12H, CH_3); ^{13}C NMR (100 MHz, $CDCl_3$, 25 ºC, δ) : 155.39, 151.46, 143.49, 137.96, 133.65, 131.83, 129.77, 129.27, 129.12, 128.69, 127.48, 57.56, 25.06, 11.33; MALDI-TOF-MS (HRMS) m/z: $[M]^-$ calculated for $C_{48}H_{36}F_2N_4O_4S_3$, 866.1867; found, 866.1841.

2.3. Device fabrication

The 5 mg mL^{-1} 5 wt% F4-TCNQ doped PTAA precursor solution was prepared by dissolving PTAA and F4-TCNQ in chlorobenzene. The 0.5 mg mL^{-1} PMMA precursor solution was prepared by dissolving PMMA in ethyl acetate. The $MAPbI_3$ precursor solution was prepared by dissolving 1.037 g PbI_2 and 0.376 g MAI (PbI_2: MAI molar ratio = 1:1.05) into 1.35 mL DMF and 0.15 mL DMSO mixed solvent. The 2FBT2NDI precursor solutions of different concentrations were prepared by dissolving 2FBT2NDI in chlorobenzene. The 10

mg mL^{-1} PCBM precursor solution was prepared by dissolving PCBM in chlorobenzene. The 0.7 mg mL^{-1} Bphen precursor solution was prepared by dissolving Bphen in ethanol.

The perovskite solar cells were fabricated as follows. First, the indium tin oxide (ITO) substrates (2×2 cm^2) were ultrasonically and subsequently cleaned with deionized water, acetone, and isopropanol for 15 min, respectively. Then, the substrates were dried by blowing nitrogen and then treated with O_3 plasma for 15 min before use. After that, a PTAA: F4-TCNQ precursor solution was spin-coated on the cleaned ITO at 6000 revolutions per minute (rpm) for 20 s. Then, the films were annealed at 100 °C on a hot plate for 2 min. For the deposition of the thin passivation layer, the PMMA precursor solution was spin-coated on the top of the ITO/PTAA:F4-TCNQ substrates at 6000 rpm for 20 s, and then annealed at 100 °C for 2 min. After the substrates were cooled down, the $MAPbI_3$ precursor solution was spin-coated on the ITO/PTAA:F4-TCNQ/PMMA substrates at 6000 rpm for 20 s. 2-Butanol (300 μL) was used as the antisolvent and was dropped on the wet $MAPbI_3$ precursor film atthe eighth second during the spin-coating process, and then the films were annealed at 100 °C for 10 s. The above spin-coating processes were conducted in a glove box under a nitrogen atmosphere and with a real-time humidity of <1 ppm. Finally, the perovskite films were transferred on a hot plate, first annealed in ambient air (at 100 °C, for 15 min, with a real-time humidity of 55-65%), and then annealed in DMSO atmosphere with the same temperature and time. For the DMSO atmosphere, 100 μL DMSO was dropped into a small ceramic crucible, and then a glass Petri dish was used to cover the samples and crucible. After the films were cooled down, the 2FBT2NDI precursor solution (10 mg mL^{-1}) was spin-coated on the perovskite layer at 2500 rpm for 30 s, and the PCBM precursor solution was spin-coated on the 2FBT2NDI layer at 2500 rpm for 30 s. Then, the Bphen precursor solution was spin-coated without additional annealing. The devices were completed by evaporating a 100 nm

thick aluminum film as the electrode. The active device area was set as 0.12 cm^2 (0.3×0.4 cm^2) by the overlapping area between the top Al cathode and the bottom ITO anode.

The electron-only devices for PCBM or 2FBT2NDI films were fabricated as follows. The 1.5 M ZnO precursor solution was spin-coated on the cleaned ITO at 4000 rpm for 30 s and then annealed at 200 °C for 30 min. After the films were cooled down, the 20 mg mL^{-1} PCBM or 2FBT2NDI chlorobenzene solution was spin-coated at 1000 rpm for 30 s without additional annealing. Finally, Ca (10 nm) and Al (100 nm) films were evaporated on top of the active layer as the electrode.

The electron-only devices for perovskite films were fabricated as follows. The 0.5 M SnO_2 precursor solution was spin-coated on the cleaned ITO at 2000 rpm for 30 s and then annealed at 150 °C for 30 min. The rest of the fabrication steps is similar to the fabrication of PSCs.

3. Results and Discussion

3.1. Synthesis and characterization

2FBT2NDI was synthesized as displayed in Figure 1a by Stille coupling reaction with a yield of 82%. The resulting product was fully characterized by ^1H NMR, ^{13}C NMR and HRMS, and these data are consistent with its proposed molecular structure. 2FBT2NDI exhibits excellent solubility in chloroform (over 30 mg/mL) and chlorobenzene (CB) (over 20 mg/mL) because of its linear conjugated framework and herringbone side chains. Thermal gravimetric analysis was used to investigate the thermal stability of 2FBT2NDI. The result in Figure S3 exhibited a 5% weight loss at 436 °C under a nitrogen atmosphere, which indicated that 2FBT2NDI has good thermal stability.

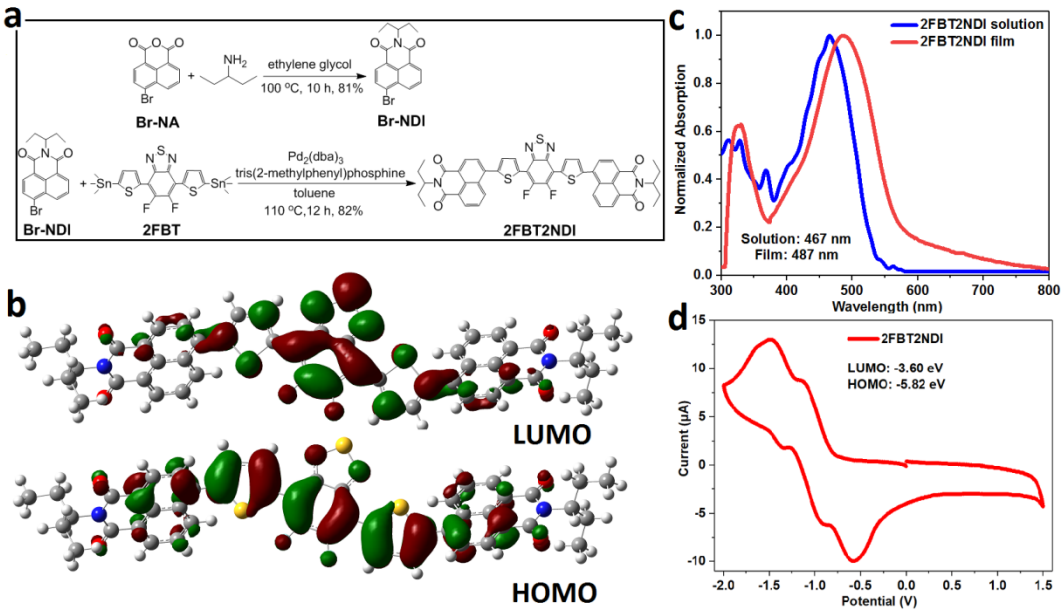

Figure 1. (a) Synthetic route of 2FBT2NDI; (b) the DFT calculations of the LUMO (top) and HOMO (bottom) electronic density distributions for 2FBT2NDI; (c) UV-Vis absorption spectra obtained in dichloromethane solution and in thin film; (d) cyclic voltammetry of 2FBT2NDI obtained in the thin film.

3.2. Optical, electrochemical and electron-transport properties

The UV-Vis absorption spectra of 2FBT2NDI in Figure 1c show absorption peak maxima at 467 nm in dichloromethane solution with a ε of 2.65×10^4 M^{-1} cm^{-1} and 487 nm in the thin film, respectively. From the absorption onset in solution, the material's optical gap (E_g) was calculated to be 2.22 eV. These results indicate that the absorption peak maxima of 2FBT2NDI were red shifted by 20 nm, demonstrating the presence of strong intermolecular interactions in the solid state because of the intermolecular hydrogen bonds and F···F interactions. Cyclic voltammetry (CV) was used to estimate the material's electrochemical properties (Figure 1d). 2FBT2NDI has two pairs of reversible reduction peaks and no oxidation peaks in the CV sweep, and the onset reduction potential is at -1.48 V for 2FBT2NDI in the film state. Moreover, the half-wave potential of the onset reduction peak

was used to calculate the LUMO level of 2FBT2NDI. As a result, the LUMO level of 2FBT2NDI was estimated to be -3.60 eV in the thin film as shown in Figures 1d, which closes to the LUMO of the $MAPbI_3$ perovskite, and thus 2FBT2NDI as the interfacial material with spike structure can reduce interfacial traps and carrier recombination [21]. According to E_g and the LUMO level, the HOMO of 2FBT2NDI was calculated to be -5.82 eV. In order to further explore the electronic density and energy levels of 2FBT2NDI, the ground-state geometries were optimized by DFT calculations as shown in Figure 1b. It is seen that both HOMO and LUMO electronic densities are located on the bisfluorobenzothiadiazole-dithiophene unit, indicating that this group is a stronger electron withdrawing group than NDI units. The calculated HOMO and LUMO levels are -5.72 and -3.18 eV, respectively, which are relatively consistent with the CV data.

Space charge limited current (SCLC) data for PCBM and 2FBT2NDI were measured to estimate the electron transport properties [22, 23], and the structure of the electron-only device was ITO/ZnO/PCBM or 2FBT2NDI/Ca/Al. As shown in Figure S5, high electron mobilities of 1.22×10^{-3} cm^2 V^{-1} s^{-1} for PCBM and 1.15×10^{-3} cm^2 V^{-1} s^{-1} for 2FBT2NDI were obtained, indicating that 2FBT2NDI has similar electron mobility to that of PCBM. These results show that 2FBT2NDI has the potential to be used as an electron transport material in the photovoltaic field.

3.3. Performance of perovskite solar cells

To investigate 2FBT2NDI as a interfacial layer for inverted PSCs, the devices were utilized with a structure of ITO/PTAA:F4-TCNQ/PMMA/$MAPbI_3$/2FBT2NDI/PCBM/Bphen /Al, as shown in Figure 3a and 3d. The devices without a 2FBT2NDI layer served as a reference. In these devices, PTAA and F4-TCNQ were used as the hole transport material and p-type doping material, respectively. F4-TCNQ-doped PTAA dissolved in CB was spin-coated onto an ITO substrate. Furthermore, to improve the device performance, PMMA was

used as the passivation layer at the hole transport layer/$MAPbI_3$ interface, and 4,7-diphenyl-1,10-phenanthroline (Bphen) served as a thin buffer layer [24]. $MAPbI_3$ was deposited in a one-step process to form a perovskite layer. Finally, either 2FBT2NDI/PCBM or PCBM was utilized as the ETL to evaluate the effect of using a 2FBT2NDI layer on the device performance.

It is necessary to investigate the efficient passivation between perovskite film and 2FBT2NDI layer, thus X-ray photoelectron spectroscopy (XPS) was applied to prove it and the results are shown in Figures 2g and S6. It is found that the Pb (4f) and I (3d) peaks of 2FBT2NDI-covered perovskite film slightly moved to the low binding energy compared with the pure perovskite, which indicates that there is an intermolecular interaction between perovskite film and 2FBT2NDI layer. In addition, the two peak positions did not change after using CB to wash the 2FBT2NDI-covered perovskite film, implying that there is a strong intermolecular interaction which ensures that 2FBT2NDI layer would not be washed off by the saturated CB solution of PCBM. This interaction would be attributed to the carbonyl and fluorine atoms of 2FBT2NDI coordinated with the Pb atoms on the surface of $MAPbI_3$ perovskite film [25-27]. Photoluminescence (PL) spectra of the pure perovskite and 2FBT2NDI-covered perovskite films were measured to further illustrate the existence of this interaction, as shown in Figure 2h. It is obvious that there are PL quenching for 2FBT2NDI-covered film and CB washed film compared with the pure perovskite film. The PL intensity of the two 2FBT2NDI-covered films can be kept nearly constant, indicating that this interaction does exist which agrees well with the XPS measurement. These results indicate that there is efficient passivation layer on the perovskite film because the saturated CB solution of PCBM cannot wash off 2FBT2NDI layer.

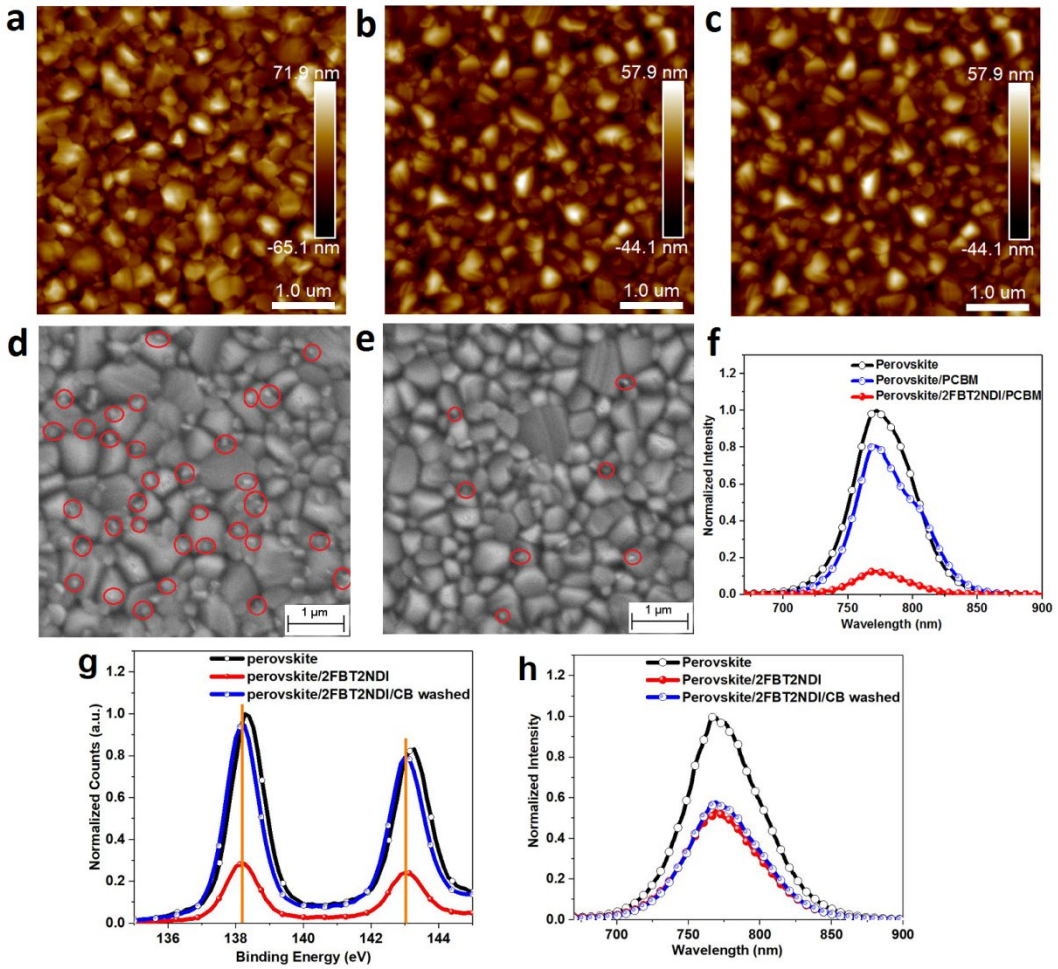

Figure 2. AFM images of the perovskite film (a) and that covered by PCBM (b) or 2FBT2NDI (c) on ITO substrates; SEM images of the perovskite films covered by PCBM (d) or 2FBT2NDI/PCBM (e) on ITO substrates and the bare PbI_2 particles marked with red circles; (f) steady-state PL spectra for perovskite films covered by PCBM or 2FBT2NDI/PCBM; (g) XPS core level spectra of Pb 4f for pure perovskite film and two 2FBT2NDI-covered perovskite films; (h) steady-state PL spectra for pure perovskite film and two 2FBT2NDI-covered perovskite films.

Atomic force microscopy (AFM) was used to investigate the surface morphologies of perovskite, PCBM-covered, and 2FBT2NDI-covered films. Figures 2a, 2b and 2c show that the bare perovskite film contains large grains with a root mean square (RMS) roughness of

18.5 nm. As expected, the film roughness significantly decreased when 2FBT2NDI or PCBM was covered on the perovskite films and both their thickness was 15 nm, which lowered the RMS roughness to 14.3 nm for PCBM and 13.1 nm for 2FBT2NDI, respectively. This indicates that the interface layer has a high coverage on the perovskite film, which makes the surface smoother to improve interfacial contact. Interestingly, the 2FBT2NDI-covered perovskite film showed a smoother surface morphology than that of PCBM, which can increase the electron extraction efficiency and reduce the contact between the perovskite layer and metal electrode. Therefore, this smooth morphology based on 2FBT2NDI-covered film can enhance the electron extraction and collection. Furthermore, Figures 2d and 2e show the scanning electron microscopy (SEM) images of perovskite films covered with PCBM or 2FBT2NDI/PCBM on the ITO substrates. Both films exhibited dense, pinhole-free morphologies, but there were still many bare PbI_2 particles on the surface of the PCBM-covered film [28]. In contrast, the PbI_2 particles on the surface of 2FBT2NDI/PCBM-covered film was significantly reduced or covered, which prevented the perovskite layer from directly contacting the metal electrode to improve the device stability. These results reveal that 2FBT2NDI can act as an efficient interface engineering to improve the photovoltaic performance and stability of PSCs.

Employing 2FBT2NDI as interface engineering, the film thickness is a key factor for achieving high-performance PSCs. Therefore, different thicknesses were prepared by changing the solution concentration and spin-coating speed to investigate how the film thickness of 2FBT2NDI affects the device performance, and the results are summarized in Table S1. Figure 3b shows that as the thickness of the 2FBT2NDI film increases, the short-circuit current density (J_{sc}) and *PCE* gradually increase. The optimal *PCE* and J_{sc} values were reached at a film thickness of 15 nm. Further increases in the film thickness caused the *PCE* and J_{sc} to gradually decrease, likely due to poor film morphology and reduced tunneling

current were detrimental to electron extraction and transport. Therefore, 15 nm was the optimal thickness when 2FBT2NDI was used as an interfacial layer.

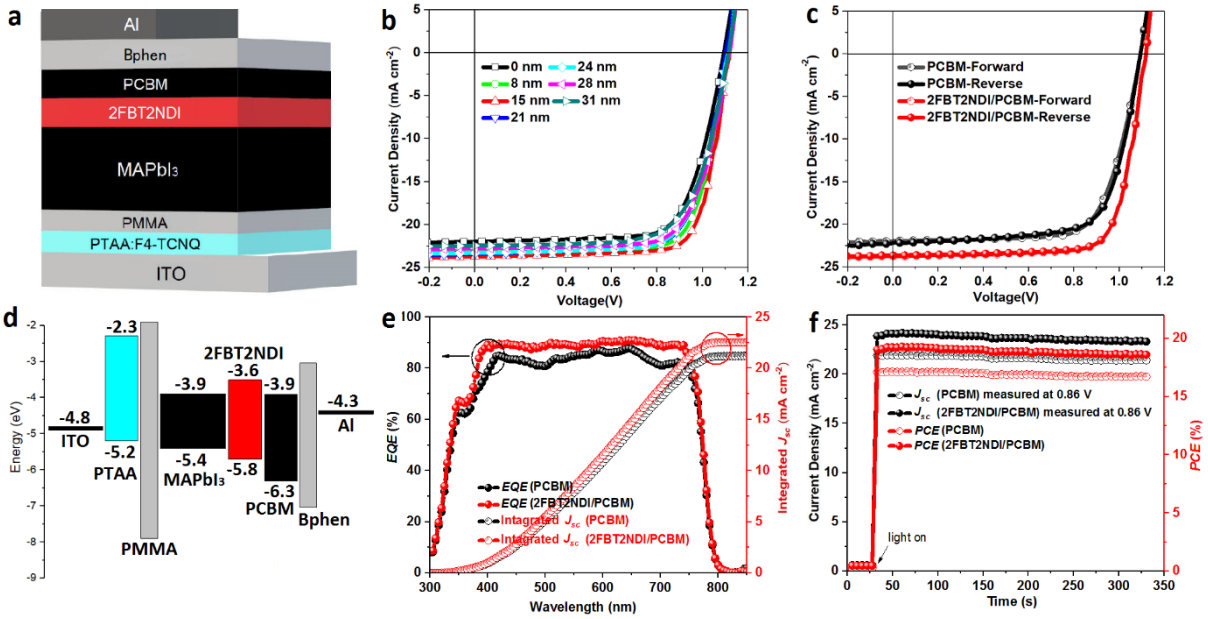

Figure 3. (a) The device structures of perovskite solar cells fabricated in this work; (b) *J-V* curves of PSCs with different thickness of the 2FBT2NDI layer; (c) forward and reverse scanning of the devices using 2FBT2NDI/PCBM or PCBM as the ETL, respectively; (d) the energy level alignments of perovskite solar cells; (e) EQE curves and the integrated J_{sc} for the 2FBT2NDI/PCBM- and PCBM-based devices; (f) stabilized photocurrent density and *PCE* output of 2FBT2NDI/PCBM- and PCBM-based devices.

The optimal devices with 2FBT2NDI layer were used to investigate the hysteresis effect of device performance, and devices without the 2FBT2NDI layer were used as the control device. These results are summarized in Table 1. Figure 3c shows there is little hysteresis for the devices without the 2FBT2NDI layer, and the hysteresis for the devices with the 2FBT2NDI layer nearly disappeared. Additionally, the control device exhibited a best *PCE* of 17.2%, with a J_{sc} of 22.0 mA cm^{-2}, an open circuit voltage (V_{oc}) of 1.09 V, and a fill factor

(*FF*) of 71.4%. The devices with 2FBT2NDI layer exhibited an improved *PCE* of 20.1%, with a higher J_{sc} (23.7 mA cm^{-2}), V_{oc} (1.11 V) and *FF* (76.3%), which demonstrates that the best *PCE* of the device with 2FBT2NDI layer is over 14% higher than that of the control device. The lower fill factor can be attributed to the smaller perovskite crystal size and some bare PbI_2 particles on the surface of perovskite films. But compared to the control device, the addition of the interfacial layer effectively improves the fill factor and PCE. To compare the hysteresis effect across two devices, a modified hysteresis index (HI) was defined in the following equation (1) [29]. The HI values were calculated to be 0.011 for the PCBM-based device and 0.0056 for the 2FBT2NDI/PCBM-based device, respectively, which demonstrates that the addition of the interfacial layer can reduce hysteresis effect. The above results indicate that the use of 2FBT2NDI as interface engineering strengthened the perovskite/ETL interfacial contact, which can passivate $MAPbI_3$ surface defects and suppress the hysteresis effect. In addition, using 2FBT2NDI as a single electron transport layer in the inverted PSCs, the device efficiency can reach to 16.0% with negligible hysteresis as shown in Figure S7, suggesting that 2FBT2NDI can be used as an electron transport layer for the PSCs. The PSCs using 2FBT2NDI as ETL were performed a bit lower in efficiency than PCBM based device because of the incomplete coverage of 2FBT2NDI on the perovskite film.

Table 1. Device performance of perovskite solar cells with or without 2FBT2NDI as an interfacial layer.

Conditions	Scan direction	J_{sc} [mA cm^{-2}]	V_{oc} [V]	*FF* [%]	*PCE* [%]
2FBT2NDI/PCBM	Forward scan	23.7	1.11	76.3	20.1
2FBT2NDI/PCBM	Reverse scan	23.7	1.12	75.9	20.1
PCBM	Forward scan	22.0	1.09	71.4	17.1
PCBM	Reverse scan	22.2	1.09	70.6	17.2

$$\mathrm{HI} = \frac{J_R(0.8\,V_{oc}) - J_F(0.8\,V_{oc})}{J_R(0.8\,V_{oc})} \quad (1)$$

The external quantum efficiency (*EQE*) curves of PSCs with or without 2FBT2NDI layer are shown in Figure 3e. The two PSCs show broad *EQE* spectra from 300-800 nm, due to the contribution of the $MAPbI_3$ layer. The *EQE* values for the device with interfacial layer were observed to be higher than those of control device, demonstrating the excellent photon harvesting and charge collection for the 2FBT2NDI-based device. Meanwhile, the integrated J_{sc} of control and 2FBT2NDI-based devices were calculated to be 21.2 mA cm^{-2} and 22.6 mA cm^{-2}, respectively, which agree with the *J-V* measurements. Figure 3f shows the steady photocurrent and *PCE* measured at the maximum power output (both 0.86 V for two devices). The steady photocurrents were 21.4 mA cm^{-2} and 23.3 mA cm^{-2}, and the stabilized *PCE*s were 16.7% and 18.6% for devices without and with 2FBT2NDI interfacial layer, respectively, which are consistent with the *J-V* measurements. These results indicate that 2FBT2NDI behaves as an efficient interface engineered material for PSCs.

To evaluate the electron transfer efficiency at the perovskite/ETL interface, PL spectra of bare perovskite, PCBM-covered and 2FBT2NDI/PCBM-covered films were measured. Figure 2f shows that, as compared with the bare perovskite film, both covered perovskite films displayed obvious PL quenching spectra. As expected, the PL quenching for the 2FBT2NDI/PCBM-covered film was more significant than that of the PCBM-covered film. These results show that the addition of the interfacial layer effectively improved the electron transfer efficiency between the perovskite film and the ETL. Time-resolved photoluminescence spectra of the perovskite films covered by PCBM or 2FBT2NDI/PCBM were measured, and the time-resolved photoluminescence decays were fitted with a biexponential decay function. The calculated decay lifetimes (Figure S8) and the fluorescence lifetime imaging microscopy images (Figures S9 and S10) are displayed. These results show that the 2FBT2NDI/PCBM-based perovskite film has a slightly lower fast-decay lifetimes

comdpared with PCBM-based perovskite film. It indicates that the addition of the 2FBT2NDI layer can increase efficient electron extraction.

To further demonstrate the effect of the 2FBT2NDI layer, SCLC measurement was used to explore the trap density (N_{trap}) and electron mobility (μ_e) of perovskite films with the electron-only device structures of ITO/SnO_2/$MAPbI_3$/2FBT2NDI/PCBM/Bphen/Al, using the devices without a 2FBT2NDI layer as the reference. The current density-voltage traces are shown in Figure 4a, and the calculation results are summarized in Table 2. Figure 4a shows three different dependence regions: an ohmic region (pink lines) at low bias, a trap-filling region beginning at V_{TFL} (trap-filled limit voltage) (blue lines), and a SCLC region occurring at a high bias (green lines). At first, V_{TFL} can be directly obtained from the intersection of the extrapolated lines in the ohmic and TFL regions. From the second region, the N_{trap} in the perovskite film was calculated by the law (2). A lower trap density was obtained for the 2FBT2NDI/PCBM-covered perovskite film (1.46×10^{15} cm^{-3}) compared with the PCBM-covered perovskite film (2.39×10^{15} cm^{-3}), indicating that using 2FBT2NDI as an interfacial layer can suppress charge-trapped recombination at the perovskite/ETL interface. At last, the electron mobility in the perovskite film was calculated from the third region according to the Mott-Gurney law (3). The 2FBT2NDI/PCBM-covered perovskite film exhibited electron mobility of 0.030 cm^2 V^{-1} s^{-1}, which was higher than the PCBM-covered perovskite film (0.019 cm^2 V^{-1} s^{-1}), suggesting that the 2FBT2NDI layer can enhance the electron extraction and transport. Therefore, superior photovoltaic performance was observed in PSCs that the device with efficient interface engineering compared with the control device.

$$V_{TFL} = \frac{eN_{trap}L^2}{2\varepsilon\varepsilon_0} \quad (2)$$

$$\mu = \frac{8J_D L^3}{9\varepsilon\varepsilon_0 V^2} \quad (3)$$

To ensure the reliability of measurements, the *PCE* statistical distribution histograms for control and 2FBT2NDI-modified in forty devices are displayed in Figure 4b. The standard deviation values of the two devices are quite reasonable, suggesting that the measurement results are reliable, and the device fabrication steps are repeatable. The devices with 2FBT2NDI layer exhibited a higher *PCE* of 19.4±0.4% than that of the control devices (17.0±0.4%), which was consistent with the *J-V* measurements. By comparing our work with records reported in the literature [30-42], a statistical diagram of the *PCE* is given in Figure 4c. It is obvious that the *PCE* (20.1%) in this work is one of the highest records for NDI-based PSCs, which imply that 2FBT2NDI as interface engineering can improve device performance.

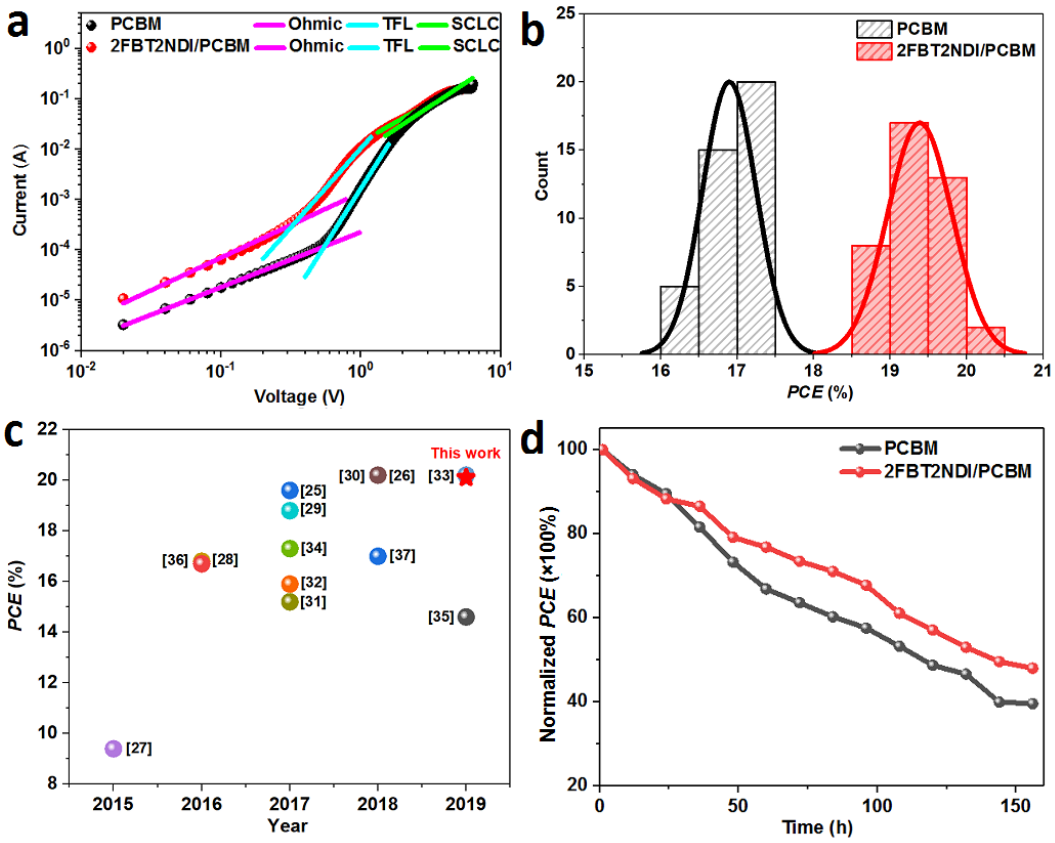

Figure 4. (a) Current density-voltage traces of the devices with or without 2FBT2NDI as the ETL by space charge limited current method; (b) *PCE* histograms of PSCs based on PCBM (40 devices) or 2FBT2NDI/PCBM (40 devices) as the ETL; (c) the *PCE* of NDI-based PSCs

reported in the literature [30-42]; (d) stability measurement of the devices under 25% humidity condition.

Table 2. Trap density and electron mobility of the devices with or without 2FBT2NDI as an interfacial layer.

Conditions	V_{TFL} [V]	N_{trap} [cm^{-3}]	μ_e [$cm^2\ V^{-1}\ s^{-1}$]
2FBT2NDI/PCBM	0.33	1.46×10^{15}	0.030
PCBM	0.55	2.39×10^{15}	0.019

The effect of the 2FBT2NDI layer on the stability of PSCs was evaluated in detail by storing the encapsulated devices under the ambient atmosphere with 25% humidity condition. Figure 4d shows the time evolution of the *PCE* values of two devices, and the *PCE* values for two devices were significantly lower after 150 hours likely due to the accelerated perovskite decomposition caused by aluminum electrode. In the first 24 hours, the *PCE* values of two devices decreased by 20%. However, the stability of the device with the 2FBT2NDI layer was higher than that of the control device from 24 to 150 hours because of full coverage and pinhole-free film obtained by using interface engineering, which is in accordance with the SEM and AFM measurements results. In addition, the amino and fluorine atoms of 2FBT2NDI could form hydrogen bonds to restrain the invading water and neutralize the migrating iodide ions, which prevents degradation of the perovskite film and improves device stability [43]. Therefore, the water contact angles for PCBM- or 2FBT2NDI-covered perovskite films were measured as shown in Figure S11. The 2FBT2NDI-covered film has a larger contact angle than the PCBM-covered film, indicating that 2FBT2NDI is more hydrophobic than PCBM, and thus a better PSC stability can be achieved using the 2FBT2NDI layer [44].

4. Conclusion

In summary, a simple NDI dimer containing a bisfluorobenzothiadiazole-dithiophene unit (2FBT2NDI) was synthesized by simple Stille coupling with a high yield. 2FBT2NDI shows excellent thermal stability and high electron mobility because of its fluorine-substituted linear conjugated framework. Moreover, 2FBT2NDI exhibits excellent film coverage and strong interactions with perovskite film, and indicating that it is suitable for use as an interfacial material spike structure in inverted PSCs. Due to efficient electron extraction, negligible hysteresis effect, and decreased charge-trapped recombination, the devices using 2FBT2NDI as interface engineering exhibited the best *PCE* of 20.1%, which was over 14% higher than that of the control devices. Therefore, the 2FBT2NDI layer can simultaneously achieve efficient surface passivation and electron extraction. The interface engineered configuration shows obvious advantages over the control device, and can potentially be applied to commercialize the inverted PSCs. The strategy used to construct the fluorine-substituted NDI dimer provides an excellent way to explore efficient interfacial materials for high-performance PSCs.

Supporting Information

Supporting Information is available from the ELSEVIER.

Acknowledgements

This work has been partially supported by the National Key R&D Program of China (2018YFC0910602); the National Natural Science Foundation of China (61775145, 61525503, 61620106016, 61835009, 81727804, 61804099); the China Postdoctoral Science Foundation Funded Project (2018M643147, 2018M643178); (Key) Project of Department of Education of Guangdong Province (2015KGJHZ002, 2016KCXTD007); and Shenzhen Basic

Research Project (JCYJ20170412110212234, JCYJ20170412105003520). W.-Y.W. would like to thank Science, Technology and Innovation Committee of Shenzhen Municipality (JCYJ20170303160036674); the Hong Kong Research Grants Council (PolyU 123384/16P, C5037-18G); Hong Kong Polytechnic University (1-ZE1C) and Ms. Clarea Au (847S) for the financial support.

Conflict of Interest

The authors declare no conflict of interest.

References

[1] H. Li, C. Chen, J. Jin, W. Bi, B. Zhang, X. Chen, L. Xu, D. Liu, Q. Dai, H. Song, Near-infrared and ultraviolet to visible photon conversion for full spectrum response perovskite solar cells, Nano Energy 50 (2018) 699-709.

[2] T. Gatti, E. Menna, M. Meneghetti, M. Maggini, A. Petrozza, F. Lamberti, The renaissance of fullerenes with perovskite solar cells, Nano Energy 41 (2017) 84-100.

[3] Z. H. Bakr, Q. Wali, A. Fakharuddin, L. Schmidt-Mende, T. M. Brown, R. Jose, Advances in hole transport materials engineering for stable and efficient perovskite solar cells, Nano Energy 34 (2017) 271-305.

[4] C. Odabasi, R. Yildirim, Performance analysis of perovskite solar cells in 2013-2018 using machine learning tools, Nano Energy, 56 (2019) 770-791.

[5] J. You, Z. Hong, Y. Yang, Q. Chen, M. Cai, T. B. Song, C. C. Chen, S. Lu, Y. Liu, H. Zhou, Y. Yang, Low-temperature solution-processed perovskite solar cells with high efficiency and flexibility, ACS Nano 8 (2014) 1674-1680.

[6] J. H. Heo, H. J. Han, D. Kim, T. K. Ahn, S. H. Lm, Hysteresis-less inverted $CH_3NH_3PbI_3$ planar perovskite hybrid solar cells with 18.1% power conversion efficiency, Energy Environ. Sci. 8 (2015) 1602-1608.

[7] J. Seo, S. Park, Y. C. Kim, N. J. Jeon, J. H. Noh, S. C. Yoon, S. Seok, Benefits of very thin PCBM and LiF layers for solution-processed p-i-n perovskite solar cells, Energy Environ. Sci. 7 (2014) 2642-2646.

[8] H. S. Jung, N. G. Park, Perovskite solar cells: from materials to devices, small 11 (2015) 10-25.

[9] Y. J. Hwang, T. Earmme, B. A. E. Courtright, F. N. Eberle, S. A. Jenekhe, n-Type semiconducting naphthalene diimide-Perylene diimide copolymers: controlling crystallinity, blend morphology, and compatibility toward high-performance all-polymer solar cells, J. Am. Chem. Soc. 137 (2015) 4424-4434.

[10] J. Yuan, W. Ma, High efficiency all-polymer solar cells realized by the synergistic effect between the polymer sidechain structure and solvent additive, J. Mater. Chem. A 3 (2015) 7077-7085.

[11] J. Zhang, H. Xiao, X. Zhang, Y. Wu, G. Li, C. Li, X. Chen, W. Ma, Z. Bo, 1,8-Naphthalimide-based nonfullerene acceptors for wide optical band gap polymer solar cells with an ultrathin active layer thickness of 35 nm, J. Mater. Chem. C 4 (2016) 5656-5663.

[12] H. F. Higginbotham, P. Pander, R. Rybakiewicz, M. K. Etherington, S. Maniam, M. Zagorska, A. Pron, A. P. Monkman, P. Data, Triphenylamine disubstituted naphthalene diimide: elucidation of excited states involved in TADF and application in near-infrared organic light emitting diodes, J. Mater. Chem. C 6 (2018) 8219-8225.

[13] W. Zhang, H. Wang, J. Miao, Y. Zhu, M. U. Ali, T. Xu, L. Zhao, D. Zhang, G. He, H. Meng, Revealing the influence of hole injection material's molecular orientation on OLED's performance, Org. Electron. 59 (2018) 301-305.

[14] M. Chen, J. Li, X. Jiao, X. Yang, W. Wu, C. R. McNeill, X. Gao, Enantiopure versus racemic naphthalene diimide-based n-type organic semiconductors: effect on charge transport, J. Mater. Chem. C 7 (2019) 2659-2665.

[15] L. Zhang, Z. Wang, C. Duan, Z. Wang, Y. Deng, J. Xu, F. Huang, Y. Cao, Conjugated polymers based on thiazole flanked naphthalene diimide for unipolar n-type organic field-effect transistors, Chem. Mater. 30 (2018) 8343-8351.

[16] X. Zhao, A. Facchetti, S. Barlow, T. J. Marks, M. A. Ratner, M. R. Wasielewski, S. R. Marder, Rylene and related diimides for organic electronic, Adv. Mater. 23 (2011) 268-284.

[17] Y. Zhao, Y. Guo, Y. Liu, 25th Anniversary article: recent advances in n-type and ambipolar organic field-effect transistors, Adv. Mater. 25 (2013) 5372-5391.

[18] S. Mathew, A. Yella, P. Guo, R. H. Baker, B. F. E. Curchod, N. A. Astani, I. Tavernelli, U. Rothlisberger, M. K. Nazeeruddin, M. Grätzel, Dye-sensitized solar cells with 13% efficiency achieved through the molecular engineering of porphyrin sensitizers, Nat. Chem. 6 (2014) 242-247.

[19] H. Zhou, L. Yang, A. C. Stuart, S. C. Price, S. Liu, W. You, Development of fluorinated benzothiadiazole as a structural unit for a polymer solar cell of 7% efficiency, Angew. Chem. Int. Ed. 50 (2011) 2995-2998.

[20] D. Dang, Y. Zhi, X. Wang, B. Zhao, C. Gao, L. Meng, A1-A-A1 type small molecules terminated with naphthalimide building blocks for efficient non-fullerene organic solar cells, Dyes Pigm. 137 (2017) 43-49.

[21] G. Kapil, T. S. Ripolles, K. Hamada, Y. Ogomi, T. Bessho, T. Kinoshita, J. Chantana, K. Yoshino, Q. Shen, T. Toyoda, T. Minemoto, T. N. Murakami, H. Segawa, S. Hayase, Highly efficient 17.6% tin-lead mixed perovskite solar cells realized through spike structure, Nano Lett., 18 (2018) 3600-3607.

[22] H. Wang, L. Chen, Y. Xiao, Constructing a donor-acceptor linear conjugation structure for heterologous perylene diimides to greatly improve the photovoltaic performance, J. Mater. Chem. C, 7 (2019) 835-842.

[23] H. Wang, Q. Fan, L. Chen, Y. Xiao, Amino-acid ester derived perylene diimides electron acceptor materials: an efficient strategy for green-solvent-processed organic solar cells, Dyes Pigm., 164 (2019) 384-389.

[24] F. Zhang, J. Song, R. Hu, Y. Xiang, J. He, Y. Hao, J. Lian, B. Zhang, P. Zeng, J. Qu, Interfacial passivation of the p-doped hole-transporting layer using general insulating polymers for high-performance inverted perovskite solar cells, Small 14 (2018) 1704007.

[25] J. Zhang, Y. Li, J. Huang, H. Hu, G. Zhang, T. Ma, P.C. Chow, H. Ade, D. Pan, H. Yan, Ring-fusion of perylene diimide acceptor enabling efficient nonfullerene organic solar cells with a small voltage loss, J. Am. Chem. Soc. 139 (2017) 16092-16095.

[26] S. Fu, X. Li, L. Wan, Y. Wu, W. Zhang, Y. Wang, Q. Bao, J. Fang, Efficient passivation with lead pyridine-2-carboxylic for high-performance and stable perovskite solar cells, Adv. Energy Mater. (2019) 1901852.

[27] H. Wang, F. Yang, Y. Xiang, S. Ye, X. Peng, J. Song, J. Qu, W. Y. Wong, Achieving efficient inverted perovskite solar cells with excellent electron transport and stability by employing a ladder-conjugated perylene diimide dimer, J. Mater. Chem. A 7 (2019) 24191-24198.

[28] F. Yang, P. Zhang, M. A. Kamarudin, G. Kapil, T. Ma, S. Hayase, Addition effect of pyreneammonium iodide to methylammonium lead halide perovskite-2D/3D heterostructured perovskite with enhanced stability, Adv. Funct. Mater. (2018) 1804856.

[29] K. Wang, Y. Shi, B. Li, L. Zhao, W. Wang, X. Wang, X. Bai, S. Wang, C. Hao, T. Ma, Amorphous inorganic electron-selective layers for efficient perovskite solar cells: feasible strategy towards room-temperature fabrication, Adv. Mater. 28 (2016) 1891-1897.

[30] J. H. Heo, S. C. Lee, S. K. Jung, O. P. Kwon, S. H. Im, Efficient and thermally stable inverted perovskite solar cells by introduction of non-fullerene electron transporting materials, J. Mater. Chem. A 5 (2017) 20615-20622.

[31] S. K. Jung, J. H. Heo, D. W. Lee, S. C. Lee, S. H. Lee, W. Yoon, H. Yun, S. H. Im, J. H. Kim, O. P. Kwon, Nonfullerene electron transporting material based on naphthalene diimide small molecule for highly stable perovskite solar cells with efficiency exceeding 20%, Adv. Funct. Mater. 28 (2018) 1800346.

[32] W. Wang, J. Yuan, G. Shi, X. Zhu, S. Shi, Z. Liu, L. Han, H. Q. Wang, W. Ma, Inverted planar heterojunction perovskite solar cells employing polymer as the electron conductor, ACS Appl. Mater. Interfaces 7 (2015) 3994-3999.

[33] Z. Zhu, C. C. Chueh, G. Zhang, F. Huang, H. Yan, A. K. Y. Jen, Improved ambient-stable perovskite solar cells enabled by a hybrid polymeric electron-transporting layer, ChemSusChem, 9 (2016) 2586-2591.

[34] C. Y. Chang, B. C. Tsai, M. Z. Lin, Y. C. Huang, C. S. Tsao, An integrated approach towards the fabrication of highly efficient and long-term stable perovskite nanowire solar cells, J. Mater. Chem. A 5 (2017) 22824-22833.

[35] X. Zhao, L. Tao, H. Li, W. Huang, P. Sun, J. Liu, S. Liu, Q. Sun, Z. Cui, L. Sun, Y. Shen, Y. Yang, M. Wang, Efficient planar perovskite solar cells with improved fill factor via interface engineering with graphene, Nano Lett. 18 (2018) 2442-2449.

[36] T. Jia, C. Sun, R. Xu, Z. Chen, Q. Yin, Y. Jin, H. L. Yip, F. Huang, Y. Cao, Naphthalene diimide based n-type conjugated polymers as efficient cathode interfacial materials for polymer and perovskite solar cells, ACS Appl. Mater. Interfaces 9 (2017) 36070-36081.

[37] D. Li, C. Sun, H. Li, H. Shi, X. Shai, Q. Sun, J. Han, Y. Shen, H. L. Yip, F. Huang, M. Wang, Amino-functionalized conjugated polymer electron transport layers enhance the UV-photostability of planar heterojunction perovskite solar cells, Chem. Sci. 8 (2017) 4587-4594.

[38] S. K. Jung, J. H. Heo, D. W. Lee, S. H. Lee, S. C. Lee, W. Yoon, H. Yun, D. Kim, J. H. Kim, S. H. Im, O. P. Kwon, Homochiral asymmetric-shaped electron-transporting materials for efficient non-fullerene perovskite solar cells, ChemSusChem 12 (2019) 224-230.

[39] S. Peng, J. Miao, I. Murtaza, L. Zhao, Z. Hu, M. Liu, T. Yang, Y. Liang, H. Meng, W. Huang, An efficient and thickness insensitive cathode interface material for high performance inverted perovskite solar cells with 17.27% efficiency, J. Mater. Chem. C 5 (2017) 5949-5955.

[40] W. Yan, Z. Wang, Y. Gong, S. Guo, J. Jiang, J. Chen, C. Tang, R. Xia, W. Huang, H. Xin, Naphthalene-diimide selenophene copolymers as efficient solution-processable electron-transporting material for perovskite solar cells, Org. Electron. 67 (2019) 208-214.

[41] C. Sun, Z. Wu, H. L. Yip, H. Zhang, X. F. Jiang, Q. Xue, Z. Hu, Z. Hu, Y. Shen, M. Wang, F. Huang, Y. Cao, Amino-functionalized conjugated polymer as an efficient electron transport layer for high-performance planar-heterojunction perovskite solar cells, Adv. Energy Mater. 6 (2016) 1501534.

[42] H. Kim, M. J. Kim, K. Choi, C. Lim, Y. H. Kim, S. K. Kwon, T. Park, Improving the performance and stability of inverted planar flexible perovskite solar cells employing a novel NDI-based polymer as the electron transport layer, Adv. Energy Mater. 8 (2018) 1702872.

[43] S. Wang, H. Chen, J. Zhang, G. Xu, W. Chen, R. Xue, M. Zhang, Y. Li, Y. Li, Targeted therapy for interfacial engineering toward stable and efficient perovskite solar cells, Adv. Mater. (2019) 1903691.

[44] K. Jiang, F. Wu, H. Yu, Y. Yao, G. Zhang, L. Zhu, H. Yan, A perylene diimide-based electron transport layer enabling efficient inverted perovskite solar cells, J. Mater. Chem. A 6 (2018) 16868-16873.